Carlos J. Cobos* and Adela E. Croce

Theoretical Kinetics Study of the Reactions Forming the ClCO Radical Cycle in the Middle Atmosphere of Venus

DOI 10.1515/zpch-2015-0608
Received March 31, 2015; accepted July 28, 2015

Abstract: A quantum-chemistry and kinetics study of key chemical reactions involved in the ClCO radical cycle of the Venus atmosphere: $Cl + CO + M \rightarrow ClCO + M$ (1); $ClCO + O_2 + M \rightarrow ClC(O)OO + M$ (2) and $ClC(O)OO + Cl \rightarrow CO_2 + ClO + Cl$ (3) ($M = CO_2$), has been performed at 150–300 K. Unimolecular reaction rate theories on potential energy features derived at the G4//B3LYP/6-311+G(3df) ab initio composite level were employed. Limiting low pressure rate coefficients calculated for Reaction (1) are in good agreement with recommended experimental values. The present results validate rate coefficient values measured for Reaction (2) over relevant strato-mesosphere Venusian conditions. Rate coefficients calculated by the SACM/CT for Reaction (3) are given by $k_3 = 2.5 \times 10^{-11} (T/300)^{0.5}$ cm^3 molecule^{-1} s^{-1}. In the absence of experimental data, these values provide the first reliable prediction for k_3.

Keywords: ClCO Cycle, Venus Atmospheric Chemistry, Ab Initio Calculations, SACM/CT Calculations.

Dedicated to Prof. Dr. Dr. h.c. mult. Jürgen Troe on the occasion of his 75th birthday

***Corresponding author: Carlos J. Cobos,** Instituto de Investigaciones Fisicoquímicas Teóricas y Aplicadas (INIFTA), Departamento de Química, Facultad de Ciencias Exactas, Universidad Nacional de La Plata, Casilla de Correo 16, Sucursal 4, La Plata (1900), Argentina, e-mail: cobos@inifta.unlp.edu.ar
Adela E. Croce: Instituto de Investigaciones Fisicoquímicas Teóricas y Aplicadas (INIFTA), Departamento de Química, Facultad de Ciencias Exactas, Universidad Nacional de La Plata, Casilla de Correo 16, Sucursal 4, La Plata (1900), Argentina

1 Introduction

The Venus atmosphere is mostly composed by CO_2 (96.5%), small concentrations of N_2 and only traces of the HCl, CO, H_2O, SO, SO_2, OCS and O_2 molecules [1–9]. At the surface the pressure is close to 96 bar and, due to strong greenhouse effects, the temperature is close to 735 K. A particular characteristic of the atmosphere is the thick sulfuric acid clouds with concentration close to 85% located at about 40–60 km which divide the low to the middle atmosphere and deplete the H_2O above this height. In this last region, the strato-mesosphere (60–100 km), the CO_2 is photodissociated by the < 227 nm solar radiation generating CO and O atoms. The reverse recombination process is spin forbidden and consequently slow. Therefore, in the absence of other loss processes, the O atoms finally combine to form O_2. This mechanism leads to CO and O_2 column abundances orders of magnitude larger than the observed [6, 10]. For this reason, chlorine catalytic cycles of chlorine containing compounds have been proposed to explain the CO and O_2 measured abundances and to account for the small extent of CO_2 decomposition [2, 3]. The cycle driven by the chloroformyl radicals, ClCO, is assumed the main mechanism for CO and O_2 consumption and CO_2 balance in the Venusian chemistry

$$\mathrm{Cl} + \mathrm{CO} + M \rightarrow \mathrm{ClCO} + M \tag{1}$$

$$\mathrm{ClCO} + \mathrm{O_2} + M \rightarrow \mathrm{ClC(O)OO} + M \tag{2}$$

$$\mathrm{ClC(O)OO} + \mathrm{Cl} \rightarrow \mathrm{CO_2} + \mathrm{ClO} + \mathrm{Cl} \tag{3}$$

$$\mathrm{ClO} + \mathrm{O} \rightarrow \mathrm{Cl} + \mathrm{O_2}, \tag{4}$$

being the net reaction $O + CO \rightarrow CO_2$. The third-body species M is predominantly CO_2. The peroxychloroformyl radical, ClC(O)OO, formed in Reaction (2) and subsequently depleted in Reaction (3), has been isolated and characterized in cryogenic matrix studies [10]. Reaction (4) is the most studied kinetic process of the cycle, being over the 200–300 K range the recommended rate coefficient $k_4 = 2.8 \times 10^{-11} \exp(85\,\mathrm{K/T})\ \mathrm{cm^3\ molecule^{-1}\ s^{-1}}$ [11]. It should be noted that, although this cycle has been considered for several years, none of the chlorine bearing species has yet been observed in the Venus atmosphere.

The recombination Reaction (1) and the reverse dissociation process ClCO+ $M \rightarrow$ Cl + CO + M(−1) are central to establish the ClCO concentration of this labile radical (the Cl–CO bond dissociation enthalpy at 0 K is $6.9 \pm 0.7\ \mathrm{kcal\,mol^{-1}}$ [12]) in the Venus stratosphere. The measured low pressure rate coefficients for CO/N_2 mixtures at 185–260 K are $k_{1,0} = [CO/N_2]\ 1.05 \times 10^{-34} \exp[810\,\mathrm{K/T}]\ \mathrm{cm^3\ molecule^{-1}\ s^{-1}}$ and $k_{-1,0} = [CO/N_2]4.1 \times 10^{-10} \exp[-2960\,\mathrm{K/T}]\ \mathrm{s^{-1}}$ [12]. The $k_{1,0}$ value agrees very well with more recent room

temperature determinations [13]. The recommended equilibrium constant at 200–300 K, $K_C = k_{-1,0}/k_{1,0} = 2.9 \times 10^{24} \exp[-3730\ \mathrm{K/T}]$ molecule cm^{-3} [11] is based on the results of Ref. [12].

Reaction (2) is a key process of the Venus chemistry. A room temperature rate coefficient value of 4.3×10^{-13} cm^3 molecule^{-1} s^{-1} has been determined by a relative rate technique at 760 Torr [13]. This value is somewhat smaller than the derived at $[CO_2] = 2.46 \times 10^{19}$ molecule cm^{-3} with the empiric Equation (5)

$$k_2 = [CO_2]5.7 \times 10^{-15} \exp\left(500\ \mathrm{K/T}\right)/(1 \times 10^{17} + 0.05\ \mathrm{cm^3\ molecule^{-1}}\ [CO_2])\ \mathrm{cm^3\ molecule^{-1}\ s^{-1}} \quad (5)$$

of 5.6×10^{-13} cm^3 molecule^{-1} s^{-1} [3]. However, neither validity ranges of temperature and pressure for Equation (5), nor experimental details have been reported. Nevertheless, this expression has been amply used by the Venus modelers [8, 9]. The oxidation pathway (2), instead of the originally suggested process $ClCO + O_2 \rightarrow CO_2 + ClO$ [1], has been confirmed by steady-state photochemical studies of $Cl_2/CO/O_2/N_2$ mixtures at 300 K [14]. Verification of Equation (5) and the assessment of its uncertainties have been claimed [6].

In addition to Reaction (3), alternative bimolecular reactions of ClC(O)OO with H, O, SO and SO_2 species have been included in modeling simulations [8, 9]. However, a sensitivity analysis indicates that Reaction (3) is the most important process. In the absence of experimental or theoretical information, a temperature independent rate coefficient of 1×10^{-11} cm^3 molecule^{-1} s^{-1} has been assumed for k_3 [3, 8, 9]. It should be noted that the concerted process (3) or the sequential process formed by reaction $ClC(O)OO + Cl \rightarrow ClCO_2 + ClO$ followed by the decomposition of the vibrationally excited $ClCO_2$ radical, $ClCO_2 \rightarrow Cl + CO_2$ might play a role.

The importance of the subject for understanding the dynamics of the Venus stratosphere, and the limited kinetic information for the elemental processes involved in the ClCO catalytic cycle, motivate the present theoretical investigation of Reactions (1)–(3). To our knowledge, this is the first quantum-chemical and kinetics study for these processes.

2 Computational details

The hybrid functional B3LYP [15–17] combined with the extended 6-311+G(3df) triple split valence basis set [18] was employed to derive optimized molecular structures and harmonic vibrational frequencies along the minimum energy pathways of the studied reactions. At the calculated structures, potential energy curves

were then obtained using the CBS-Q//B3LYP/6-311+G(3df) [19] and G4//B3LYP/6-311+G(3df) quantum-chemical models [20]. In addition, the composite W1BD model was used to study Reaction (1) [21, 22]. Because all models lead to similar potentials curves, for a sake of simplicity, only the kinetic results derived with the best model, G4//B3LYP/6-311+G(3df), are reported here.

The Synchronous Transit-Guided Quasi-Newton (STQN) method was employed to locate transition structures [23, 24], and the Intrinsic Reaction Coordinate (IRC) method to verify their connectivity with reactants and products [25, 26]. All calculations were performed using the Gaussian 09 software package [27].

Well-established models developed by Troe have been employed in this paper. Limiting low and high pressure rate coefficients and falloff curves were calculated employing the unimolecular reaction rate theory. Strong collision low pressure rate coefficients, k_0^{SC}, were estimated using a factorized model [28, 29], For the high pressure rate coefficients, k_∞, the statistical adiabatic channel model/classical trajectory (SACM/CT) formulation for the atom + linear rotor reaction type was employed [30]. The pressure dependence of the association rate coefficients was modeled with the recently formulated reduced falloff curves method [31]. In all these calculations, theoretical molecular information provided by the present quantum-chemical results was employed. Finally, energy resolved microcanonical rate coefficients for tight processes involved in the analysis of Reaction (3) were estimated using the inverse Laplace transform method [32].

3 Quantum-chemical calculations

Specific rotational effects relevant in both the low and the high pressure regions of barrierless recombination reactions depend significantly on the shape (interfragment separation range) and the well depth of the isotropic/radial electronic potential. On the other hand, the anisotropic part of the potential energy surface accounts for the hindrance in the rate coefficients. These last effects, mostly manifest in k_∞, are exclusively attributed to the evolution of the degrees of freedom orthogonal to the reaction coordinate along the minimum energy path (MEP). For these reasons, quantum-chemical calculations of these regions of the electronic potential were performed. The close relationship between some selected gas-phase reactions and their potential energy surfaces has been recently exemplified [33].

Figure 1 shows the potential energy curves computed along the MEP for the ClCO → Cl+CO process at the G4//B3LYP/6-311+G(3df) composite level. The cal-

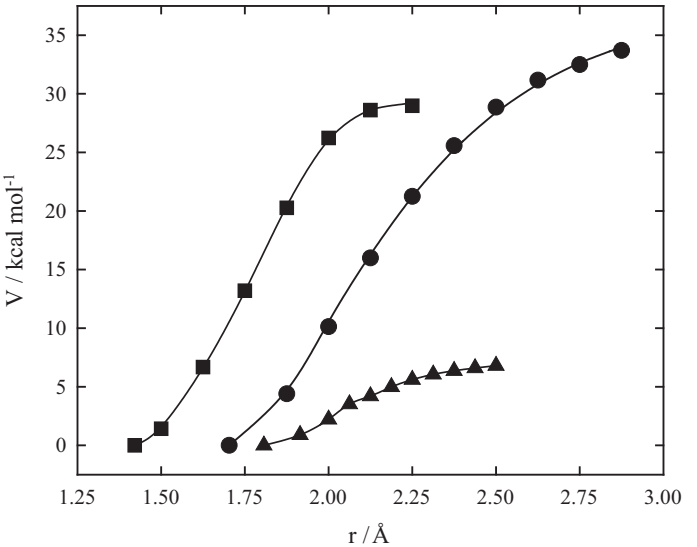

Figure 1: Potential energy curves for ClCO → Cl + CO (▲), ClC(O)OO → ClCO + O_2 (■), and ClC(O)OOCl → ClC(O)OO + Cl (●) calculated along the MEP at the G4//B3LYP/6-311+G(3df) level. The solid lines are fits with Morse functions using the parameters given in Table 1.

Table 1: Morse parameters employed to fit the ab initio potential energy curves.
[a] B3LYP/cc-PVTZ+d calculations.

Level of theory	D_e (kcal mol^{-1})	r_e (Å)	β (Å^{-1})
ClCO → Cl + CO			
CBS-Q//B3LYP/6-311+G(3df)	7.7	1.807	4.28
G4//B3LYP/6-311+G(3df)	6.5	1.807	5.03
W1BD	6.9	1.818[a]	4.76
ClC(O)OO → ClCO + O_2			
CBS-Q//B3LYP/6-311+G(3df)	29.3	1.421	$3.65 - 4.96(r - r_e) + 12.45(r - r_e)^2$
G4//B3LYP/6-311+G(3df)	29.5	1.421	$4.68 - 13.55(r - r_e) + 28.57(r - r_e)^2$
ClC(O)OOCl → ClC(O)OO + Cl			
CBS-Q//B3LYP/6-311+G(3df)	39.9	1.703	2.38
G4//B3LYP/6-311+G(3df)	37.8	1.703	2.52

culated values can be very well fitted using the standard Morse expression $V(r) = D_e[1 - \exp(-\beta(r - r_e))]^2$ with a bond dissociation energy of $D_e = 6.5$ kcal mol^{-1}, a range parameter of $\beta = 5.03$ Å^{-1}, and an equilibrium bond length for Cl–CO of $r_e = 1.807$ Å. A similar fit quality was obtained with the CBS-Q//B3LYP/6-

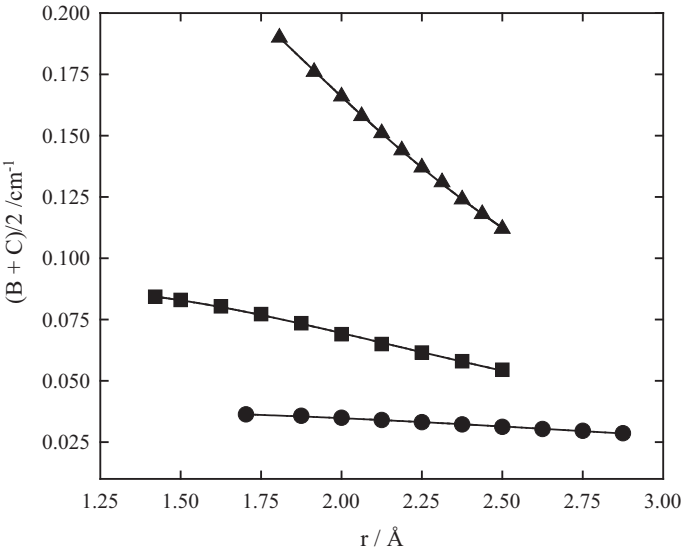

Figure 2: Effective rotational constants for ClCO → Cl + CO (▲), ClC(O)OO → ClCO + O_2 (■), and ClC(O)OOCl → ClC(O)OO + Cl (●) calculated along the MEP at the B3LYP/6-311+G(3df) level. The solid lines are fits with the function $B_{\text{eff}}(r) = a_0/[1 + a_1(r - r_e) + a_2(r - r_e)^2]$ using the a_i parameters given in the text.

311+G(3df) and W1BD composite models. The resulting Morse parameters are listed in Table 1. In a similar way, the potentials for the Reactions (2) and (3) were investigated. The results are depicted in Figure 1 and Table 1. The shape of the potential profile along the MEP for the ClC(O)–OO bond can only be well reproduced with a C–O bond length-dependent Morse parameter, $\beta(r) = \beta_0 + \beta_1(r - r_e) + \beta_2(r - r_e)^2$. A similar behavior has been found for the related FC(O)–OO radial potential [34].

To characterize the centrifugal barriers, effective rotational constants, $B_{\text{eff}}(r) = [B(r) + C(r)]/2$, along the MEP obtained from computed B3LYP/6-311+G(3df) structures were derived and fitted with the expression $B_{\text{eff}}(r) = a_0/[1 + a_1(r - r_e) + a_2(r - r_e)^2]$ [35]. The results for the ClCO, ClC(O)OO, and ClC(O)OOCl species are illustrated in Figure 2. The a_i parameters are given below.

As mentioned above, the anisotropy of the potential accounts for the evolution of the transitional vibrational frequencies with the interfragment distance. The data corresponding to the ClCO bending mode (Reaction 1) and to the torsional and bending modes assigned to the ClC(O)OO–Cl bond (Reaction 3) are depicted in Figure 3. The observed exponential decays of these vibrational modes

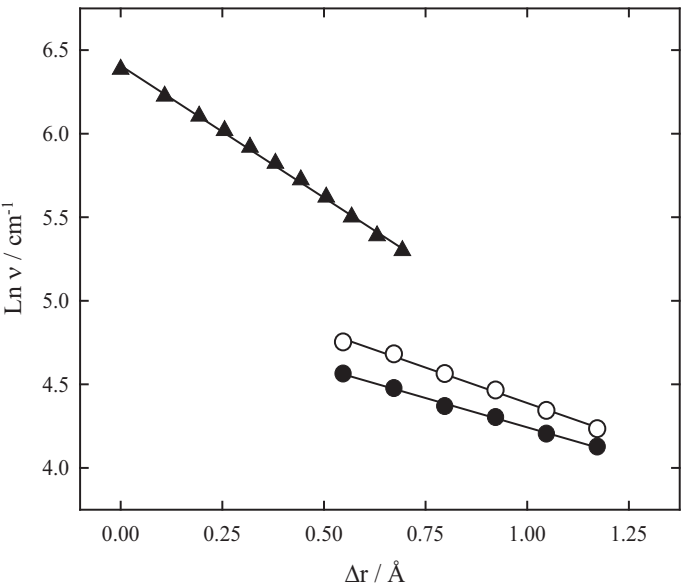

Figure 3: Harmonic vibrational frequencies for ClCO → Cl + CO (▲: bending) and ClC(O)OOCl → ClC(O)OO + Cl (○: torsion; ●: bending) calculated along the MEP at the B3LYP/6-311+G(3df) level. $\Delta r = r - r_e$, with equilibrium bond distances of 1.807 Å (Cl–CO) and 1.703 Å (ClC(O)OO–Cl). The looseness parameters α derived from linear regressions, from top to bottom, are 1.59, 0.85, and 0.70 Å^{-1}.

agree with the simple functional dependence, $\nu \approx \exp[-\alpha(r - r_e)]$, proposed by Quack and Troe forty years ago [36]. For the bending of ClCO, a value $\alpha = 1.59$ Å^{-1} was obtained while for the torsional and bending modes of ClC(O)OOCl, values of 0.85 and 0.70 Å^{-1} were found. These anisotropy parameters are in reasonable agreement with those derived by fitting experimental k_∞ values with a simplified SACM [37]. The harmonic vibrational frequencies and rotational constants for the molecules involved in the kinetic modeling are given in Table 2.

Many bimolecular reactions proceed *via* complex-forming processes [38]. Well known examples are the important O + OH → HO_2^* → H + O_2 and OH + CO → HOCO* → H + CO_2 reactions [38–40]. As Figures 1 and 4 show, a barrierless capture process initially generates a ground-state vibrationally excited bound complex ClC(O)OOCl* in Reaction (3). Afterwards, it can be either collisionally stabilized by the bath gas forming a thermalized ClC(O)OOCl adduct (the G4//B3LYP/6-311+G(3df) trans → cis electronic barrier for isomerization is 0.7 kcal mol^{-1}) or, alternatively decompose to the final Cl + CO_2 + ClO prod-

Table 2: Harmonic wavenumbers and rotational constants calculated for the species in Reactions (1) to (3) at the B3LYP/6-311+G(3df) level.

Species	Harmonic wavenumbers (cm^{-1})	Rotational constants (cm^{-1})
O_2	1645	1.456
CO	2170	1.930
ClO	861	0.619
CO_2	679, 679, 1374, 2414	0.392
ClCO	355, 592, 1944	5.310, 0.194, 0.187
ClC(O)O	280, 427, 642, 655, 1123, 1389	0.459, 0.175, 0.127
ClC(O)OO (trans)	133, 288, 405, 498, 621, 800, 918, 1128, 1913	0.327, 0.0950, 0.0736
ClC(O)OOCl (trans)	72, 90, 274, 323, 447, 489, 661, 697, 821, 862, 1003, 1895	0.219, 0.0374, 0.0353
TS1	125i, 14, 63, 106, 121, 223, 336, 480, 643, 860, 1320, 2323	0.151, 0.0287, 0.0241
TS2	207i, 17, 142, 229, 290, 455, 475, 693, 717, 970, 1284, 1522	0.259, 0.0376, 0.0329

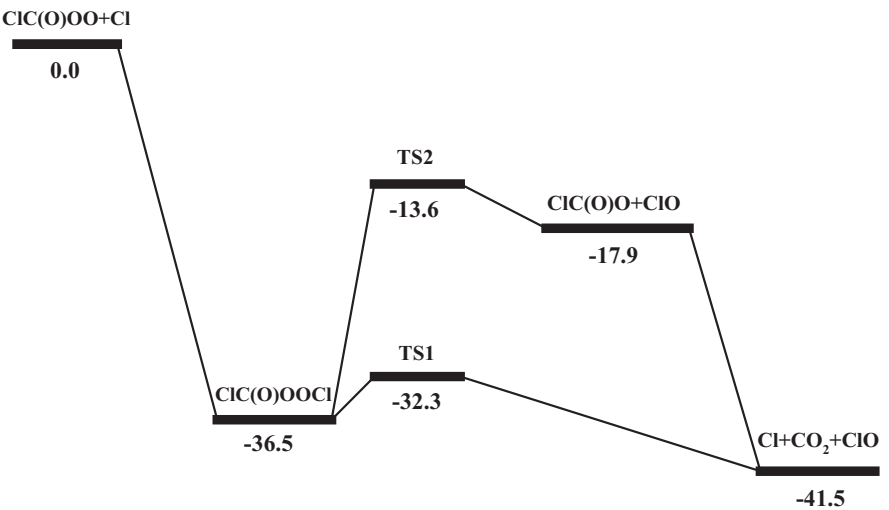

Figure 4: Schematic energy diagram for Reaction (3) obtained at 0 K from G4//B3LYP/6-311+G(3df) calculations. Energy values in $kcal\ mol^{-1}$.

ucts through the TS1 or TS2 transition states. These species were characterized by STQN and IRC calculations. Their molecular properties are listed in Table 2.

4 Kinetic calculations

To characterize the influence of a given chemical reaction on the species concentration profiles, the so called column reaction rate, $CR = \int k(h)(1 + h/R_0)^2 dh$ (where $k(h)$ is the rate coefficient as a function of the altitude h, and $R_0 = 6052$ km is the Venus surface radius), and the mean altitude, $h_m = (1/CR) \int k(h)(1 + h/R_0)^2 h dh$, are frequently employed by the modelers [9]. These are useful magnitudes to investigate the balance of species and provide quantitative evaluations of chemical processes. As can be observed, both quantities are directly proportional to the reaction rate coefficient values, and, therefore, reliable kinetic information as a function of the altitude (i.e., as a function of the temperature, and eventually total pressure) is required for their estimation. The CR and h_m values reported in the present study have been computed by Krasnopolsky [9] using the 47.5 and 111.5 km values for the integration limits.

4.1 Limiting rate coefficients for Reaction (1)

Reaction (1) is expected to be close to the third-order regime over all Venusian conditions. The low pressure rate coefficients reported at 185–260 K, $k_{1,0} = [CO/N_2]1.05\times10^{-34} \exp[810\ K/T]\ cm^3\ molecule^{-1}$, have been mostly employed by the modelers [12]. The estimated CR values for this process are between 4.1×10^{12} and $5.1 \times 10^{15}\ cm^{-2}\ s^{-1}$ and the mean altitude lies in the strato-mesosphere, $h_m = 71$ km [9]. To illustrate the importance of Reaction (1), it should be noted than only 12 of the 153 reactions (photochemical and thermal) proposed to model the Venus atmosphere between 47 and 112 km, exhibit CR values larger than the above lower limit, and only the reverse dissociation process (−1) has a value identical to this upper limit [9].

Here we have compared the experimental kinetic data [12] with predicted strong collision low pressure rate coefficients evaluated as in Refs. [28] and [29]

$$k_0^{SC} = (1/K_c)[M]Z_{LJ}(\rho_{vib,h}(E_0)kT/Q_{vib}) \exp(-E_0/kT)F_E F_{anh} F_{rot} \qquad (6)$$

These rate coefficients account for the established equilibrium populations of metastable molecular configurations below the reaction threshold energy $E_0 = 6.9$ kcal mol^{-1} [12]. We have obtained a similar value of 7.1 kcal mol^{-1} with the W1BD composite model [21, 22].

Here Z_{LJ} is the Lennard–Jones collision frequency between the excited adduct ClCO and $M = CO_2$, $\rho_{vib,h}(E_0)$ is the harmonic vibrational density of states, F_E takes into consideration the energy dependence of $\rho_{vib,h}(E_0)$, F_{anh} accounts for

anharmonicity, F_{rot} for rotational effects, Q_{vib} is the ClCO vibrational partition function and K_c is the equilibrium constant. The mathematical expressions for the different factors in Equation (6) are given elsewhere [28, 29]

The molecular parameters for the ClCO Lennard–Jones potential were estimated from molecular critical properties [41]. The resulting values based on the Cl_2CO molecule are $\sigma = 4.1$ Å and $\varepsilon/k = 340$ K. For CO_2, the parameters $\sigma = 3.943$ Å and $\varepsilon/k = 200.9$ K were employed [42]. To compute F_{rot}, the threshold $E_0(J)$ energies were derived from the maxima of the centrifugal potentials $V_{cent}(r) = V(r) + B_{eff}(r)[J(J+1)]$, where $B_{eff}(r) = 0.190/[1 + 0.658(r - 1.807) + 0.489(r - 1.807)^2]$ cm^{-1} with r in Å, and $V(r)$ is the expression obtained from the G4//B3LYP/6-311+G(3df) quantum-chemical calculations (Table 1). The derived centrifugal barriers depend on the rotational quantum number J and can be fitted using the two-parameter formula $E_0(J) \approx E_0(J=0) + C_\nu[J(J+1)]^{1/\nu}$ [29, 35] with $C_\nu = 2.29 \times 10^{-2}$ cm^{-1} and $\nu = 1.16$. The K_C values of Nicovich et al. were employed in Equation (6) [11, 12]. The resulting k_0^{SC} values are very well reproduced by the Equation (7)

$$k_{0,1}^{SC} = [CO_2]4.6 \times 10^{-31}(T/300)^{-4.0} \exp(-584\ \mathrm{K/T})\ \mathrm{cm^3\ molecule^{-1}\ s^{-1}} \quad (7)$$

over the 150–300 K range. Employing the experimental value determined for $M = CO_2$ at 214 K (which is a factor of 3.2 larger than those measured for $M = CO/N_2$), $k_{0,1} = 1.5 \times 10^{-32}$ cm^3 molecule^{-1} s^{-1} [12] and our predicted k_0^{SC} of 1.2×10^{-31} cm^3 molecule^{-1} s^{-1}, a collisional efficiency of $\beta_c(CO_2) = k_{0,1}/k_{0,1}^{SC} \approx 0.13$ results. Following now the simple expression which connects β_c with the average energy transferred (in all up and down transitions) between energized ClCO radicals and CO_2, $-\langle\Delta E\rangle \approx F_E kT\beta_c/(1 - \beta_c^{1/2})$ [43], we roughly estimate $-\langle\Delta E\rangle \approx 33$ cm^{-1}. This small value is consistent with those measured in direct collisional energy transfer experiments for triatomic molecules at low excitation energy levels [44–46]. Assuming, as usual, an almost temperature independent $-\langle\Delta E\rangle$, β_c values ranging from about 0.18 and 0.10 are calculated between 150 and 300 K. Then, the predicted $k_{0,1}$ results,

$$k_{0,1} = [CO_2]5.4 \times 10^{-32}(T/300)^{-5.1} \exp(-645\ \mathrm{K/T})\ \mathrm{cm^3\ molecule^{-1}\ s^{-1}} \quad (8)$$

The ClCO cycle operates efficiently in the 67–90 km altitude region, where the CO_2 photolysis is the largest and the temperature decreases from about 240 to 170 K. At 240 K, the calculated rate coefficient is almost 30% larger than the experimental value which is based on the temperature independent scaling ratio between the CO_2 and CO/N_2 colliders of 3.2. On the other hand, at 170 K the theoretical value is 50% smaller than the experimental one. Considering the the-

oretical and, in less extension, the experimental uncertainties, the agreement is reasonably good.

The kinetics at the high pressure regime is dominated by the intramolecular time evolution of molecules excited above the reaction threshold. The present reaction exhibits a potential energy curve with a smooth transition between the CO rotational motion of the reagent and the ClCO bending mode. The SACM/CT is an appropriate tool to predict k_∞ for this kind of reactions [30]. It has been demonstrated that the high pressure rate coefficients can be factorized as $k_\infty = f_{\text{rigid}} k_\infty^{\text{PST}}$ [37]. Here k_∞^{PST} is the phase space theory rate coefficient computed with the isotropic part of the potential, and f_{rigid} is a rigidity factor that accounts for dynamical constraints arising from the anisotropy of the potential energy surface. The first factor is given by

$$k_\infty^{\text{PST}} = (kT/h)(h^2/2\pi\mu kT)^{3/2} f_{\text{el}} Q_{\text{cent}} \tag{9}$$

where μ denotes the reduced mass of the collision pair for the A + B + → C reaction, $f_{\text{el}} = Q_{\text{el,C}}/Q_{\text{el,A}}Q_{\text{el,B}}$ the electronic degeneracy factor and $Q_{\text{cent}} = \Gamma(1 + 1/\nu)(kT/C_\nu)^{1/\nu}$ the centrifugal pseudo-partition function [35].

In the SACM/CT framework, the rigidity factor for a reaction between an atom and a linear molecule forming a nonlinear adduct is given by [30]

$$f_{\text{rigid}}(T \to 0) \approx (1 + Z^2 + Z^8)^{-1/8} \tag{10}$$

$$Z = (C/3\sin^2\gamma_e)^n/\gamma_1 \tag{11}$$

and

$$C = [\varepsilon(r_e)]^2/2BD_e \tag{12}$$

Here, n and γ_1 are parameters which depend on γ_e, the angle of the molecule at the potential minimum. Anisotropy effects are accounted for by Equation (12), where $\varepsilon(r_e)$ is the vibrational frequency of the bending mode of the adduct and B the rotational constant of the reactant fragment. This expression is valid for a potential parameter ratio of $\alpha/\beta = 0.5$ [37]. For other cases, as the present $\alpha/\beta = 0.32$, a modified equation for C applies: $C_{\text{eff}} = CF(kT/De)^{2\alpha/\beta-1}$ with $F = 1 - 0.7(2\alpha/\beta - 1) + (2\alpha/\beta - 1)^2$. After transforming the computed $f_{\text{rigid}}(T \to 0)$ into center-of-mass coordinates and correcting by small temperature dependencies the rigidity factor f_{rigid} is obtained [30]. The resulting k_∞^{PST} and f_{rigid} values for Reaction (1) were found almost temperature independent between 150 and 300 K. In fact, k_∞^{PST} values between 9.87×10^{-11} and 1.25×10^{-10} cm^3 molecule^{-1} s^{-1} and f_{rigid} values between 0.10 and 0.11 were calculated. Finally, the computed high pressure rate coefficients can be represented as

$$k_{\infty,1} = 1.4 \times 10^{-11}(T/300)^{0.5} \text{ cm}^3 \text{ molecule}^{-1} \text{ s}^{-1} \tag{13}$$

The magnitude of $k_{\infty,1}$ and its temperature dependence is typical for this type of reactions [11, 40].

The limiting rate coefficients allow to characterize the center of the falloff curve, $[M]_c = k_\infty/k_0$. This corresponds to the bath gas concentration for which the extrapolated k_0 would be equal to k_∞. At relevant atmospheric temperatures, between 170 and 240 K, the concentration derived from Equations (8) and (13) is between $[CO_2]_c = 4.8 \times 10^{20}$ molecule cm^{-3} (11 bar) and 1.1×10^{21} molecule cm^{-3} (36 bar). These pressures are much higher than those prevailing in the region where the ClCO cycle is more important, 4×10^{-4} and 0.1 bar and, therefore, the termolecular process is the only one of importance.

4.2 Rate coefficients for Reaction (2)

The dominant pathway for CO_2 production in the Venus atmosphere is Reaction (2) followed by Reaction (3). Based on rate coefficients estimated with Equation (5), the values CR = 3.5×10^{12} cm^{-2} s^{-1} and $h_m = 74$ km have been estimated [9]. Due to the fact that the applicability ranges of Equation (5) are not clear, a confrontation against theoretical results seems to be interesting.

The ClC(O)OO radical exhibits more vibrational modes and a larger threshold energy than the ClCO radical. Therefore, falloff effects are expected to be present in the recombination Reaction (2) at the prevailing Venus atmosphere. To analyse this reaction, the above formulation for k_0 was applied [28, 29]. For the present case, an additional factor that takes into account the ClC(O)–OO torsional mode (the G4//B3LYP/6-311+G(3df) rotational barrier is 5.6 kcal mol^{-1}), $F_{\text{rot int}}$, must be included in Equation (6). For the σ and ε/k parameters of ClC(O)OO, estimated values of 4.7 Å and 340 K were used [41]. The centrifugal barriers employed to calculate F_{rot} were derived using the expression $B_{\text{eff}}(r) = 0.0843/[1 + 0.198(r - 1.421) + 0.295(r - 1.421)^2]$ cm^{-1}. The remaining input data are listed in Tables 1 and 2. For these calculations the computed equilibrium constant $K_C = 9.4 \times 10^{26} \exp(-13\,400\ \text{K/T})$ molecule cm^{-3} was employed. The resulting k_0^{SC} rate coefficients are very well represented between 150 and 300 K by the following expression,

$$k_{0,2}^{SC} = [CO_2]8.4 \times 10^{-31}(T/300)^{-2.5} \exp(-40\ \text{K/T})\ \text{cm}^3\ \text{molecule}^{-1}\ \text{s}^{-1} \quad (14)$$

The collisional efficiency obtained at 300 K from the ratio between the experimental value $k_{0,2} = 3.0 \times 10^{-31}$ cm^3 molecule^{-1} s^{-1} [3] and $k_{0,2}^{SC} = [CO_2]$ 7.3×10^{31} cm^3 molecule^{-1} s^{-1} is $\beta_c = 0.41$. This efficiency leads to $-\langle\Delta E\rangle = 275$ cm^{-1}. This appears to be a reasonable value, and comparable to those ob-

tained in direct measurements of molecules more complex than triatomics [46]. Then, as in Section 4.1, β_c values of 0.58, 0.51, 0.46 and 0.41 were calculated at 150, 200, 250 and 300 K, respectively. The expression that represents the derived low pressure rate coefficients is

$$k_{0,2} = [CO_2]4.2 \times 10^{-31}(T/300)^{-3.3} \exp(-100\,K/T)\ cm^3\ molecule^{-1}\ s^{-1} \quad (15)$$

To explore the pressure and temperature dependencies of Reaction (2) and compare the resulting theoretical predictions with $k_{0,2}$ values obtained from expression (5), the knowledge of $k_{\infty,2}$ is required. Unfortunately, the present B3LYP/6-311+G(3df) calculations indicate that, along the MEP the four transitional modes are strongly mixed. This fact precludes a reliable estimation of their anisotropic α parameters which affects enormously the quality of the predicted f_{rigid}. Therefore, an alternative strategy was followed. To this end, the rate coefficient measured at 1 atm and 300 K by Yung and DeMore of $k = 5.6 \times 10^{-13}$ cm^3 molecule^{-1} s^{-1} [3] was fitted using the most recent formulation of the falloff curves method given by Troe and Ushakov [31]

$$k = [k_0/(1 + k_0/k_\infty)]/[1 + (k_0/k_\infty)^n]^{1/n} \quad (16)$$

Here, $n = [\ln 2/\ln(2/F_{cent})][0.8 + 0.2(k_0/k_\infty)^q]$, $q = (F_{cent} - 1)/\ln(F_{cent}/10)$ and $F_{cent} = F(k_0/k_\infty = 1) = F_{cent}^{SC} F_{cent}^{WC}$. The strong collision component of the center broadening factor F_{cent}^{SC} was calculated with the computed ClC(O)OO vibrational frequencies, while the weak collision component is simply estimated as $F_{cent}^{WC} = \beta_c^{0.14}$ [29]. In this way, using $k_{0,2} = 3.0 \times 10^{-31}$ cm^3 molecule^{-1} s^{-1} [3] and $\beta_c = 0.4$, the high pressure rate coefficient $k_{\infty,2} = 8.3 \times 10^{-13}$ cm^3 molecule^{-1} s^{-1} results. This value is comparable with those measured for the related reaction FCO + O_2 → FC(O)OO of 8.5×10^{-13} cm^3 molecule^{-1} s^{-1} (at 300 mbar of CO and 213–358 K) [47] and 1.2×10^{-12} cm^3 molecule^{-1} s^{-1} (at 1000 mbar of SF_6 and 296 K) [48]. On the other hand, photochemical studies of $Cl_2/CO/O_2/N_2$ mixtures performed at 300 K, suggest that Reaction (2) is almost pressure independent between 300 and 755 Torr. Thus, a temperature independent $k_{\infty,2} = 8.3 \times 10^{-13}$ cm^3 molecule^{-1} s^{-1} and the $k_{0,2}$ values given by Equation (15) were employed to get the falloff curves depicted in Figure 5. As can be noted, a good agreement was found between the rate coefficients at $[CO_2] \leq 10^{17}$ molecule cm^{-3}. However, at larger concentrations, a pronounced divergence between both sets of rate data is apparent. This fact is attributable to the marked negative temperature dependence of k_∞, $\approx T^{-2.4}$, predicted by Equation (5). Nevertheless, as Figure 6 shows, a reasonably good agreement is observed when the rate coefficients are represented as a function of the altitude (where the temper-

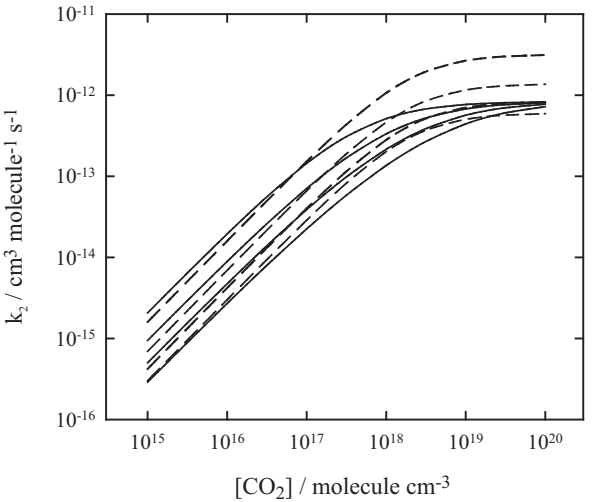

Figure 5: Falloff curves for the reaction $ClCO + O_2 + CO_2 \rightarrow ClC(O)OO + CO_2$. (- - -): Equation (5) [3]; (——): present study. Calculations, from top to bottom, at 150, 200, 250, and 300 K.

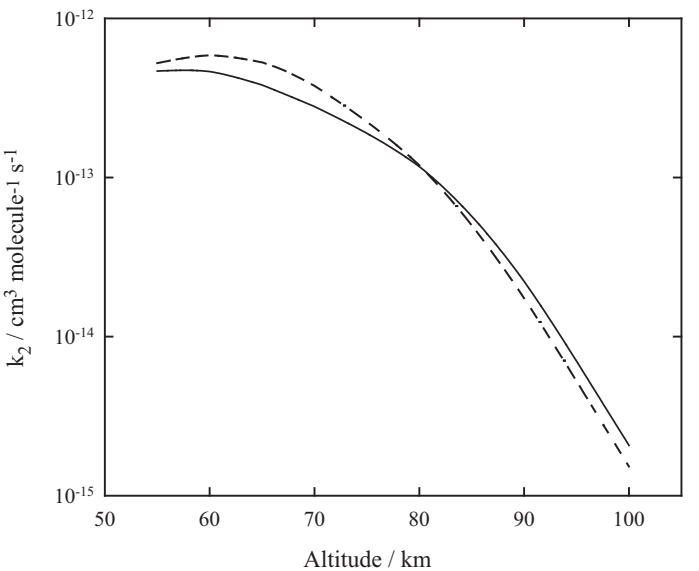

Figure 6: Rate coefficients for the reaction $ClCO + O_2 + CO_2 \rightarrow ClC(O)OO + CO_2$ as a function of the altitude above the surface of Venus. (- - -): Equation (5) [3]; (——): present study.

ature and the pressure change respectively from 300 to 160 K and from 0.5 to 3×10^{-5} bar). At 67 and 90 km our k_2 values are nearly 60% smaller and 20% larger, respectively, than those reported in Ref. [3]. This is a quite reasonable agreement that supports the k_2 values obtained with Equation (5).

4.3 Rate coefficients for Reaction (3)

According to the quantum-chemical calculations, Reaction (3) evolves on the ground-state potential energy surface of the ClC(O)OOCl molecule. From the energetic point of view, the most favored pathway for the unimolecular decomposition of this initially highly energized species is through the TS1 configuration. This is also the most feasible channel from kinetic grounds. In fact, due to the strong dependence of the specific rate coefficients, $k(E)$, on total energy E, larger $k(E)$ values are expected for the decomposition through TS1 than via TS2. Assuming that these reactions follow a simple Arrhenius behavior at the high pressure limit, a rough estimation of $k(E)$ can be done by using the inverse Laplace transform method [32] combined with the Whitten–Rabinovitch approximation for the vibrational density of states [49], $k(E) \approx A_\infty[(E-E_\infty+a(E-E_\infty)E_Z)/(E+a(E)E_Z)]^{s-1}$. The zero-point vibrational energies E_Z and the $a(E - E_\infty)$ and $a(E)$ correction factors were calculated with the vibrational frequencies listed in Table 2. The E values were taken from Figure 4. For both tight decomposition channels a pre-exponential factor of $A_\infty = 1 \times 10^{14}$ s^{-1} was assumed. The resulting microscopic rate coefficients for TS1 and TS2 are predicted to be 3×10^{13} and 5×10^{10} s^{-1}. A similar calculation indicates that the back ClC(O)OOCl redissociation to the reactants is a negligible contributing channel. Therefore, the collisional deactivation of the vibrationally excited molecules is the only competing channel. To estimate this, the deactivation rate coefficient was approached as $k_d \approx \beta_c Z_{LJ} \approx 0.4 \times 2 \times 10^{-10}$ cm^3 molecule^{-1} s^{-1} $\approx 8 \times 10^{-11}$ cm^3 molecule^{-1} s^{-1}. At average atmospheric pressures of 4×10^{-4} to 0.1 bar (1.7×10^{16} to 3.0×10^{18} molecule cm^{-3} at 170 and 240 K respectively) the resulting quenching rates of 1.4×10^6 and 2.4×10^8 s^{-1} are much smaller than the specific rate coefficients for decomposition through channel TS1 of 3×10^{13} s^{-1}. Therefore, under all practical conditions, the quasi-concerted process giving CO_2 + ClO + Cl is dominant. As a consequence, the reaction is exclusively determined by the initial capture process, and $k_3 = k_{\infty,3}$.

The rate coefficients were calculated with the SACM/CT [30] using the G4//B3LYP/6-311+G(3df) results. The potential energy surface for this reaction is characterized by a ratio $\alpha/\beta = 0.31 \pm 0.03$. Here the average of the α values found for the torsion, 0.85 Å^{-1}, and for the bending, 0.70 Å^{-1}, modes in ClC(O)OOCl

was employed (see Figure 3). As for other atom + polyatomic reactions [50–53], the ClC(O)OO radical was assumed quasi-linear with a rotational constant given by the arithmetic mean of the two smaller ClC(O)OO rotational constants, B = 0.0843 cm^{-1}. A γ_e angle of 44° was obtained from the equilibrium structure of ClC(O)OOCl. The adduct transitional frequency $\varepsilon(r_e)$ was taken as the geometrical mean of the two smaller ClC(O)OOCl vibration frequencies, 80 cm^{-1}.

Employing the rotational constants $C_\nu = 4.89 \times 10^{-3}$ cm^{-1} and $\nu = 1.13$ calculated from the centrifugal barriers computed with the expression $B_{eff}(r) = 0.0363/[1 + 0.139(r - 1.703) + 0.0778(r - 1.703)^2]$ cm^{-1}, upper bound rate coefficients of $k_{\infty,3}^{PST} = 7.4 \times 10^{-11}(T/300)^{0.4}$ cm^3 $molecule^{-1}$ s^{-1} were obtained at 150–300 K. After multiplication by f_{rigid} values of 0.31, 0.33, 0.34 and 0.35, the following equation for k_3 is obtained

$$k_3 = 2.5 \times 10^{-11}(T/300)^{0.5} \text{ cm}^3 \text{ molecule}^{-1} \text{ s}^{-1} \quad (17)$$

The above stated uncertainty of ± 0.03 units in α/β leads to an uncertainty in k_3 of about ± 12%.

The present is the first theoretical study of Reaction (3), and no experimental data are available for comparison. However, the calculated k_3 can be compared with the measured for the related reaction FC(O)OO + F → FC(O)O + FO [54]. Similar to Reaction (3), this process proceeds through an energized peroxide FC(O)OOF which afterwards dissociates to products. By contrast with Reaction (3), the large electronic barrier for the F–CO_2 bond fission of about 21 kcal mol^{-1} [55] combined with the low endothermicity of the global process, precludes its unimolecular dissociation. The measured bimolecular rate coefficient at 295 K of 4.5×10^{-12} cm^3 $molecule^{-1}$ s^{-1}, is about a factor of five smaller than the predicted for Reaction (3). This fact suggests that the motions of FC(O)O and F confined by a less attractive radial potential (β = 3.5 $Å^{-1}$, from B3LYP/6-311+G(2d) calculations [54]) lead to more hindered activated complexes.

Over the temperature of interest, the predicted k_3 values are 1.8 to 2.5 larger than the value normally employed in the modeling of the Venus´chemistry, of 1×10^{-11} cm^3 $molecule^{-1}$ s^1. This fact indicates that the estimated CR factor of 3.1×10^{12} cm^{-2} s^{-1} [9] should be increased in about a factor of two.

5 Conclusions

The present quantum-chemical and kinetics calculations support the important ClCO catalytic cycle of the Venus middle atmosphere. Reaction rate coefficients obtained for Reactions (1) and (2) are within a factor of two of the values employed

in recent modeling studies [8, 9]. In particular, the data reported for k_2 are reasonably well reproduced by the present calculations for an wide range of temperatures and pressures. Finally, a SACM/CT study based on an ab initio potential energy surface provides the first reliable estimation for k_3.

Acknowledgement: This research project was supported by the Universidad Nacional de La Plata, the Consejo Nacional de Investigaciones Científicas y Técnicas (CONICET) and the Agencia Nacional de Promoción Científica y Tecnológica. We thank to Professor Jürgen Troe for continuing support and hospitality.

References

1. V. A. Krasnopolsky and V. A. Parshev, Nature **282** (1981) 610.
2. W. D. DeMore and Y. L. Yung, Science **217** (1982) 1209.
3. Y. L. Yung and W. D. DeMore, Icarus **51** (1982) 199.
4. C. de Bergh, V. I. Moroz, F. W. Taylor, D. Crisp, B. Bézard, and L. V. Zasova, Planet. Space Sci. **54** (2006) 1389.
5. F. P. Mills and M. Allen, Planet. Space Sci. **55** (2007) 1729.
6. F. P. Mills, L. W. Esposito, and Y. L. Yung, Atmospheric Composition, Chemistry, and Clouds, in: *Exploring Venus as a Terrestrial Planet*, Geophysical Monograph Series, vol. 176, L. W. Esposito, E. R. Stofan, T. E. Cravens (Ed.), American Geophysical Union, Washington, (2007), pp. 73–100.
7. V. A. Krasnopolsky, Planet. Space Sci. **59** (2011) 952.
8. X. Zhang, M. C. Liang, F. P. Mills, D. A. Belyaev, and Y. L. Yung, Icarus **217** (2012) 714.
9. V. A. Krasnopolsky, Icarus **218** (2012) 230.
10. H. Pernice, P. Garcia, H. Willner, J. S. Francisco, F. P. Mills, M. Allen, and Y. L. Yung, P. Natl. Acad. Sci. USA **101** (2004) 14007.
11. S. P. Sander, R. R. Friedl, J. R. Barker, D. M. Golden, M. J. Kurylo, P. H. Wine, J. P. D. Abbatt, J. B. Burkholder, C. E. Kolb, G. K. Moortgat, R. E. Huie, and V. L. Orkin, *Chemical Kinetics and Photochemical Data for Use in Atmospheric Studies*, NASA/JPL Data Evaluation, JPL Publication, 06-2 Evaluation No. 17, California (2011), http://jpldataeval.jpl.nasa.gov/.
12. J. M. Nicovich, K. D. Kreutter, and P. H. Wine, J. Chem. Phys. **92** (1990) 3539.
13. A. D. Hewitt, K. M. Brahan, G. D. Boone, and S. A. Hewitt, Int. J. Chem. Kinet. **28** (1996) 763.
14. T. Ohta, B. Chem. Soc. Jpn. **56** (1983) 869.
15. A. D. Becke, J. Chem. Phys. **98** (1983) 5648.
16. A. D. Becke, Phys. Rev. A **38** (1988) 3098.
17. C. Lee, W. Yang, and R. G. Parr, Phys. Rev. B **37** (1988) 785.
18. M. J. Frisch, J. A. Pople, and J. S. Binkley, J. Chem. Phys. **80** (1984) 3265, and references therein.
19. J. A. Montgomery Jr., M. J. Frisch, J. W. Ochterski, and G. A. Petersson, J. Chem. Phys. **110** (1999) 2822.
20. L. A. Curtiss, P. C. Redfern, and K. Raghavachari, J. Chem. Phys. **126** (2007) 084108.
21. J. M. L. Martin and G. de Oliveira, J. Chem. Phys. **111** (1999) 1843.

22. E. C. Barnes, G. A. Petersson, J. A. Montgomery, M. J. Frisch, and J. M. L. Martin, J. Chem. Theory Comput. **5** (2009) 2687.
23. C. Peng and H. B. Schlegel, Israel J. Chem. **33** (1993) 449.
24. C. Peng, P. Y. Ayala, H. B. Schlegel, and M. J. Frisch, J. Comput. Chem. **17** (1996) 49.
25. K. Fukui, Accounts Chem. Res. **14** (1981) 363.
26. H. P. Hratchian and H. B. Schlegel, Find Minima, Transition States, and Following Reaction Pathways on Ab Initio Potential Energy Surfaces, in: *Theory and Applications of Computational Chemistry: The First Forty Years*, C. E. Dykstra, G. Frenking, K. S. Kim, G. Scuseria (Eds.), Elsevier, Amsterdam (2005), pp. 195–249.
27. M. J. Frisch, G. W. Trucks, H. B. Schlegel, G. E. Scuseria, M. A. Robb, J. R. Cheeseman, G. Scalmani, V. Barone, B. Mennucci, G. A. Petersson, H. Nakatsuji, M. Caricato, X. Li, H. P. Hratchian, A. F. Izmaylov, J. Bloino, G. Zheng, J. L. Sonnenberg, M. Hada, M. Ehara, K. Toyota, R. Fukuda, J. Hasegawa, M. Ishida, T. Nakajima, Y. Honda, O. Kitao, H. Nakai, T. Vreven, J. A. Montgomery, Jr., J. E. Peralta, F. Ogliaro, M. Bearpark, J. J. Heyd, E. Brothers, K. N. Kudin, V. N. Staroverov, R. Kobayashi, J. Normand, K. Raghavachari, A. Rendell, J. C. Burant, S. S. Iyengar, J. Tomasi, M. Cossi, N. Rega, J. M. Millam, M. Klene, J. E. Knox, J. B. Cross, V. Bakken, C. Adamo, J. Jaramillo, R. Gomperts, R. E. Stratmann, O. Yazyev, A. J. Austin, R. Cammi, C. Pomelli, J. W. Ochterski, R. L. Martin, K. Morokuma, V. G. Zakrzewski, G. A. Voth, P. Salvador, J. J. Dannenberg, S. Dapprich, A. D. Daniels, O. Farkas, J. B. Foresman, J. V. Ortiz, J. Cioslowski, and D. J. Fox, Gaussian 09, Revision A.02, Gaussian, Inc., Wallingford CT (2009).
28. J. Troe, J. Chem. Phys. **66** (1977) 4758.
29. J. Troe, J. Phys. Chem. **83** (1979) 114.
30. A. I. Maergoiz, E. E. Nikitin, J. Troe, and V. G. Ushakov, J. Chem. Phys. **108** (1998) 5265.
31. J. Troe and V. G. Ushakov, Z. Phys. Chem. **636** (2014) 1.
32. W. Forst, J. Phys. Chem. **76** (1972) 342.
33. J. Troe, Mol. Phys. **112** (2014) 2374.
34. J. S. Francisco and Y. Zhao, Chem. Phys. Lett. **153** (1988) 296.
35. J. Troe, J. Chem. Phys. **75** (1981) 226.
36. M. Quack and J. Troe, Ber. Bunseng. Phys. Chem. **78** (1974) 240.
37. C. J. Cobos and J. Troe, J. Chem. Phys. **83** (1985) 1010.
38. J. Troe, J. Chem. Soc. Faraday T. **90** (1994) 2303.
39. J. Troe, Ber. Bunseng. Phys. Chem. **99** (1995) 341–347.
40. D. L. Baulch, C. T. Bowman, C. J. Cobos, R. A. Cox, Th. Just, J. A. Kerr, M. J. Pilling, D. Stocker, J. Troe, W. Tsang, J. Walker, and J. Warnatz, J. Phys. Chem. Ref. Data **34** (2005) 757.
41. R. C. Reid, J. M. Prausnitz, and T. K. Sherwood, *The Properties of Gases and Liquids*, 3rd edn., McGraw-Hill, New York (1977).
42. F. M. Mourits and F. H. A. Rummens, Can. J. Chem. **55** (1977) 3007.
43. J. Troe, J. Chem. Phys. **66** (1977) 4745.
44. M. Heymann, H. Hippler, H. J. Plach, and J. Troe. J. Chem. Phys. **87** (1987) 3867.
45. M. Heymann, H. Hippler, D. Nahr, H. J. Plach, and J. Troe, J. Phys. Chem. **92** (1988) 5507.
46. H. Hippler and J. Troe, Recent Direct Studies of Energy Transfer in Vibrationally Highly Excited Molecules in the Ground Electronic State, in: *Bimolecular Collisions, Advances in Gas-Phase Photochemistry and Kinetics*, M. N. R. Ashfold, J. E. Baggott (Eds.), Royal Society of Chemistry, London (1989), pp. 209–262.
47. M. M. Maricq, J. J. Szente, G. A. Khitrov, and J. S. Francisco, J. Chem. Phys. **98** (1993) 9522.
48. T. J. Wallington, T. Ellermann, O. J. Nielsen, and J. Sehested, J. Phys. Chem. **98** (1994) 2346.

49. G. Z. Whitten and B. S. Rabinovitch, J. Chem. Phys. **38** (1963) 2466.
50. J. Hahn, K. Luther, and J. Troe, Phys. Chem. Chem. Phys. **2** (2000) 5098.
51. M. P. Badenes, A. E. Croce, and C. J. Cobos, Phys. Chem. Chem. Phys. **6** (2004) 747.
52. M. P. Badenes, A. E. Croce, and C. J. Cobos, J. Phys. Chem. A **110** (2006) 3186.
53. C. Buendía-Atencio and C. J. Cobos, J. Fluorine Chem. **132** (2011) 474.
54. M. P. Badenes, E. Castellano, C. J. Cobos, A. E. Croce, and M. E. Tucceri, Chem. Phys. **253** (2000) 205.
55. J. S. Francisco and A. N. Goldstein, Chem. Phys. **127** (1988) 73.